

Supporting Information

Thermal characterization of highly exothermic flash chemistry in a continuous flow calorimeter

Gang Fu,^[a,b] Juncheng Jiang,^[b] Christopher A. Hone^{*[a,c]} and C. Oliver Kappe^{*[a,c]}

[a] *G. Fu, Dr. C. A. Hone, Prof. Dr. C. Oliver Kappe*

Institute of Chemistry, University of Graz, NAWI Graz

Heinrichstrasse 28, A-8010 Graz (Austria)

[b] *G. Fu, Prof. Dr. J.C. Jiang*

College of Safety Science and Engineering, Nanjing Tech University, Nanjing 211816,

China

[c] *Dr. C. A. Hone, Prof. Dr. C. Oliver Kappe*

Center for Continuous Flow Synthesis and Processing (CCFLOW), Research Center

Pharmaceutical Engineering (RCPE), Inffeldgasse 13, 8010 Graz (Austria)

E-mail: christopher.hone@rcpe.at; oliver.kappe@uni-graz.at

Homepage: <http://goflow.at>

Contents

1 General information.....	4
1.1 Materials.....	4
1.2 GC-FID analysis	4
1.3 GC-MS analysis	4
2 Neutralization benchmarking.....	5
2.1 Setup for neutralization.....	5
2.2 Calorimetry data.....	5
2.2.1 Calorimetry at 25 °C	5
2.2.2 Calorimetry at 5 °C	8
3 Calorimetry for the reaction of HexLi with EtOH.....	10
3.1 General procedure for the reaction in the flow calorimeter	10
3.2 Calorimetry results in the flow calorimeter at 0 °C	10
3.3 Batch verification	14
3.3.1 General procedure	14
3.3.2 Calorimetry results in batch	14
3.3.3 Titration of 2-MeTHF with HexLi.....	16
4 Calorimetric characterization for the preparation of tertiary ester 2 and alcohol 3	17
4.1 General procedure	17
4.2 DoE data.....	17
4.2.1 DoE setup.....	17
4.2.2 DoE analysis	19
4.3 Computational fluid dynamics simulation for solvents mixing	23
4.3.1 Geometry and governing equations	23

4.3.2	Solution and boundary conditions.....	24
4.3.3	Definition of degree of mixing.....	24
4.3.4	Mesh independence.....	25
4.3.5	Mixing at different flow rates	26
4.4	Calorimetry data.....	28
4.4.1	Calorimetry for preparation of tertiary ester 2	28
4.4.2	Calorimetry for preparation of tertiary alcohol 3.....	30
5	Calorimetric characterization of Br–Li exchange and its quench with I ₂	33
5.1	General procedure	33
5.2	Calorimetry data.....	34
5.2.1	Calorimetry for Br–Li exchange.....	34
5.2.2	Calorimetry for quench of lithiated intermediate 6 with I ₂	37
	References.....	40

1 General information

1.1 Materials

Extra dry 2-MeTHF ($\geq 99\%$, stabilizer free) and extra dry hexanes ($\leq 97\%$, mixture of isomers) were purchased from Thermo Fisher Scientific. It is important that anhydrous solvents are used to minimize the influence of moisture in the reactions. Two different concentrations of HexLi solution were purchased for the project: a 2.3 M hexane solution from Sigma-Aldrich and a 2.5 M hexane solution from Thermo Fisher Scientific. Di-*tert*-butyldicarbonate (**1**) (99%) was obtained from Fluorochem. 1-Bromo-4-chlorobenzene (**5**) (99%) was purchased from Sigma-Aldrich and iodine (98%) was obtained from TCI. NaOH (99%), AcOH (99.8%) and EtOH ($> 99.7\%$) were purchased from VWR. The numbers shown in brackets correspond to the chemical purity. All chemicals were commercially available and used without further purification.

1.2 GC-FID analysis

Gas chromatography-flame ionization detection (GC-FID) analysis was performed on a Shimadzu GC FID 230 with a flame ionization detector, using a RTX-5MS column (30 m \times 0.25 mm ID \times 0.25 μ m) and helium as carrier gas (40 cm/sec linear velocity). The injector temperature was set to 280 °C. After 1 min at 50 °C, the temperature was increased by 25 °C/min to 300 °C and kept constant at 300 °C for 4 min. The detector gases used for flame ionization were hydrogen and synthetic air (5.0 quality).

1.3 GC-MS analysis

Gas chromatography-mass spectrometry (GC-MS) was performed using a Shimadzu GCMS-QP2010 SE, using an Rtx-5MS column (30 m \times 0.25 mm \times 0.25 μ m) and helium as carrier gas with a linear velocity of 40 cm/sec. The injector temperature was set to 280 °C. After 1 min at 50 °C, the oven temperature was increased by 25 °C/min to 300 °C and then kept at 300 °C for 3 min. The mass detector was a quadrupole with pre rods and electron impact ionization. The following settings were used in the detector: ion source temperature 200 °C, interface temperature 310 °C, solvent cut time 2 min 30 sec, acquisition mode scan, mass range $m/z = 50$ till $m/z = 400$.

2 Neutralization benchmarking

2.1 Setup for neutralization

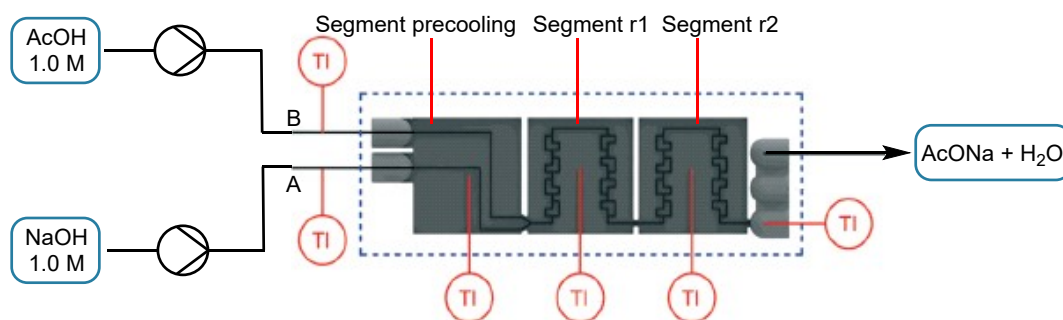


Fig. S1. Setup for AcOH – NaOH neutralization, TI stands for thermocouple.

2.2 Calorimetry data

2.2.1 Calorimetry at 25 °C

Fig. S2 shows the measured data for the neutralization performed at 25 °C. As can be observed, the temperatures measured at the inlets and outlet were close to the set temperature. The three segments were maintained at 25 °C and only a small temperature increase could be observed when the flow rates were changed. After that change, the temperatures quickly went back to the set temperature due to the PID control (Fig. S2a). The thermoelectric voltages, U_{pre} , did not change significantly as the convective heat from the two inlet streams was small. U_{r1} and U_{r2} increased immediately with the increase of flow rates and then gradually reached steady state (Fig. S2b). Besides, more reaction heat flux was transferred and detected by Seebeck elements at higher flow rates, resulting in a larger U_{r1} and U_{r2} .

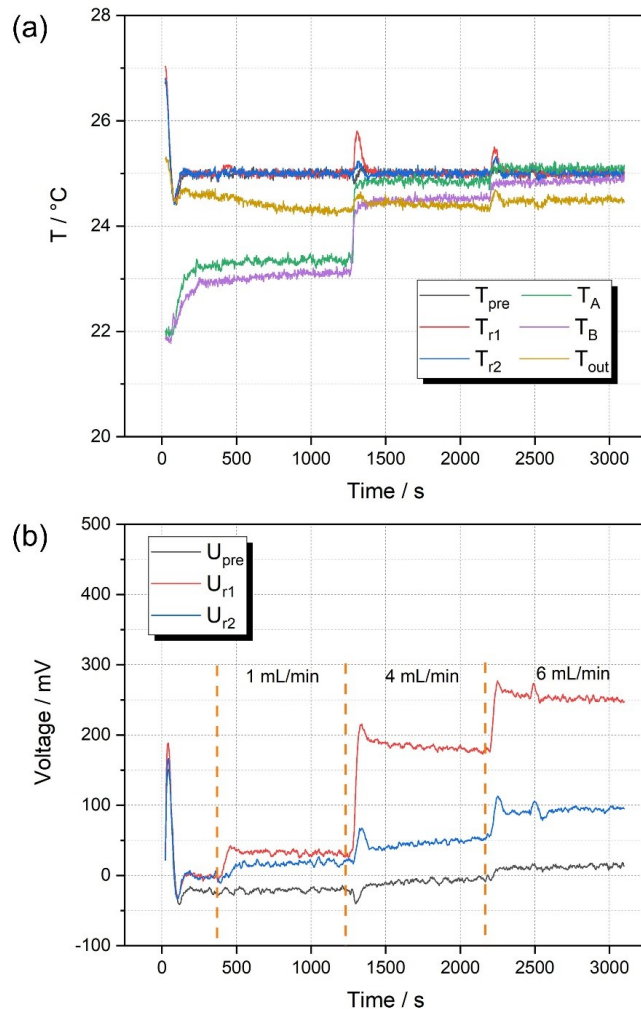


Fig. S2. Neutralization of AcOH with NaOH at 25 °C at different total flow rates: (a) temperatures at inlets (T_A , T_B), outlet (T_{out}), precooling segment (T_{pre}), r1 segment (T_{r1}) and r2 segment (T_{r2}); (b) thermoelectric voltages of precooling segment (U_{pre}), r1 segment (U_{r1}) and r2 segment (U_{r2}).

The calibration data are depicted in Fig. S3. Different voltages from 0 to 5.85 V were set to the DC power supply and the corresponding thermoelectric voltages generated by the heating foils were recorded (Fig. S3a). Similarly, the temperatures of the three segments were controlled at the set temperature, as can be seen in Fig. S3b. Then correlations between power input and thermoelectric voltage were fitted, shown in Fig. S3c.

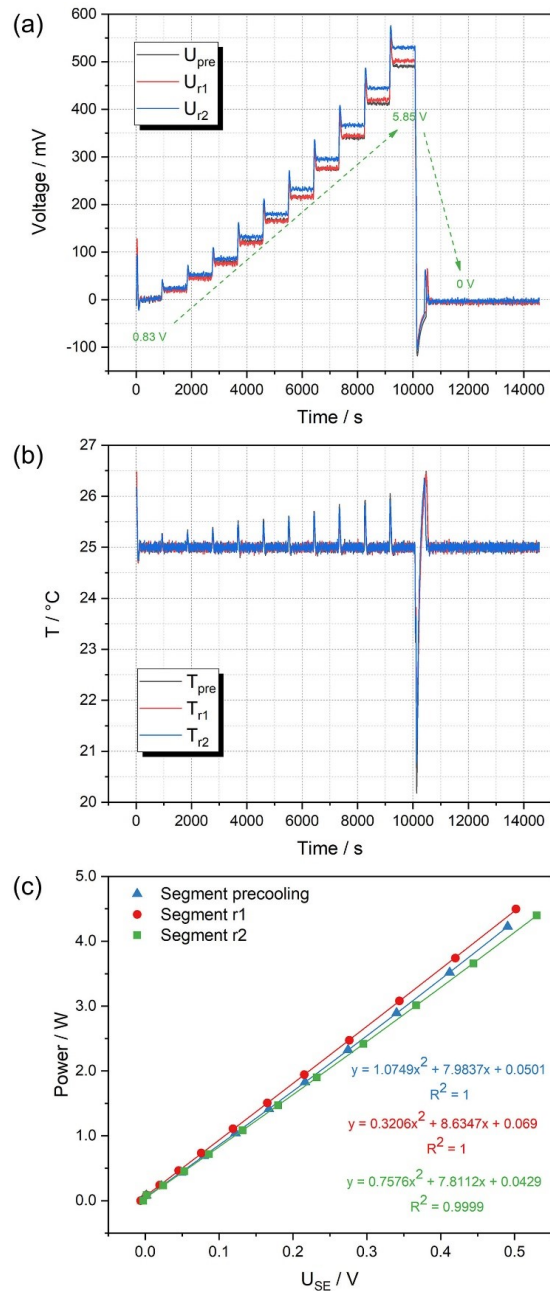


Fig. S3. Calibration of the reactor segments for neutralization at 25 °C: (a) thermoelectric voltages; (b) temperatures of the three segments; (c) correlations of heat flux and thermoelectric voltage.

With these data in hand, the reaction enthalpy was calculated and the result is given in Table S1. Compared to the enthalpy of -57.4 kJ/mol from the literature, the deviation was only 3.8% [1].

Table S1. Reaction enthalpy for neutralization at 25 °C at different flow rates.

Entry	Total flow rate [mL/min]	ΔH_r [kJ/mol]	Ave. \pm SD [kJ/mol]
1	1.0	-59.3	
2	4.0	-59.4	
3	5.0	-59.6	-59.6 ± 0.3
4	6.0	-60.0	

2.2.2 Calorimetry at 5 °C

Initially, when operating at 5 °C a much smaller enthalpy with an average of -35.7 kJ/mol was obtained following the aforementioned procedures. The reaction was repeated several times at different flow rates. However, the results were consistent. To figure out the reason for this small value, a blank test with only the solvents (water) was conducted. A comparison of thermoelectric voltages between neutralization reaction and solvents mixing is shown in Fig. S4. Since the starting solutions were at room temperature (~ 22 °C), there was a large difference between inlet temperatures and the set temperature. As a result, a large amount of convection heat was detected in the precooling segment (Fig. S4a). In the meantime, the voltages of these two processes in the precooling segment increased with the increasing of flow rates and the two curves were completely the same. In segment r1 and r2, the neutralization took place and the voltages should be much higher than the calibration line. While for the mixing, the voltages should be similar to the baseline as mixing would not generate or absorb any heat. However, the result was obviously not the case as expected in segment r1 (Fig. S4b). Therefore, the low value of reaction enthalpy was likely to result from segment r1. When calculating enthalpy, the thermoelectric voltages from the reaction were compared to the baseline (calibration at 0 V) and the power could then be obtained from the correlations. An assumption made here was that the voltages for mixing should be the same as the baseline. Since the voltages of mixing in segment r1 were lower, the part of heat between mixing curve and baseline was missed in calculation. Hence, a smaller reaction enthalpy is obtained. After we included this part of heat, it gave an average of -59.2 ± 1.1 kJ/mol, which is very close to the value measured at 25 °C. A possible explanation for this phenomenon was as follows: due to the big convection heat in the precooling segment, the corresponding Peltier element worked at a high power. Although the connection parts between three reactor segments were small, heat conduction

still existed and segments were not completely independent from each other. As a result, when the Peltier element cooled down the precooling segment, it also cooled down the r1 segment and had an influence on its voltages. As the r2 segment was far from it, this influence was negligible. Thus, the mixing curve in segment r2 was still close to the baseline. While for the neutralization at 25 °C, there was no such a problem because the convection heat was relatively small.

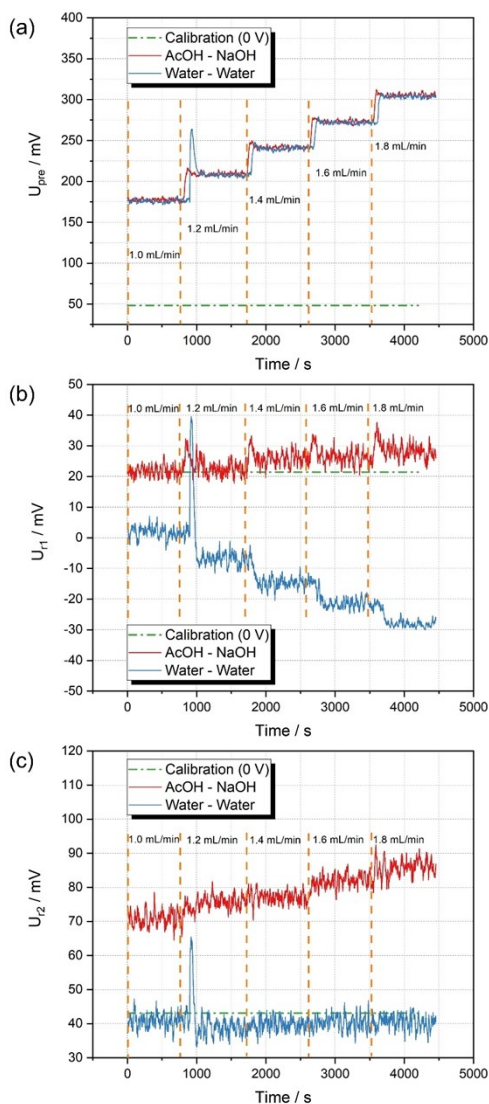


Fig. S4. Comparison of thermoelectric voltages in the three segments between neutralization reaction and solvents mixing: (a) precooling segment; (b) r1 segment; (c) r2 segment.

Table S2. Reaction enthalpy for neutralization at 5 °C at different flow rates.

Entry	Total flow rate [mL/min]	ΔH_r [kJ/mol]	Ave. \pm SD [kJ/mol]
1	1.2	-58.0	
2	1.4	-60.4	
3	1.6	-60.6	
4	1.2	-58.3	
5	1.4	-58.9	
6	1.6	-59.5	-59.2 \pm 1.1
7	1.2	-59.2	
8	1.4	-60.6	
9	1.6	-60.0	
10	1.2	-56.8	
11	1.4	-59.2	
12	1.6	-59.9	

3 Calorimetry for the reaction of HexLi with EtOH

3.1 General procedure for the reaction in the flow calorimeter

The feed solutions were kept under an inert atmosphere and introduced using syringe pumps (HiTec Zang, SyrDos2). Prior to performing the reaction, the entire system was flushed with dry 2-MeTHF and hexane for 20 min and then switched to the feed solutions. The reaction was operated for 15 min at the set temperature for each flow rate. After the reaction, dry solvents were used to run the blank test and flush the system.

3.2 Calorimetry results in the flow calorimeter at 0 °C

The calibration data at 0 °C is shown in Fig. S5. Fig. S6 shows the results for reaction (on the left) and for the solvents mixing (on the right). The temperatures for these two processes were similar and well controlled. For the reaction, U_{pre} and U_{r1} increased with increase in flow rate. While for U_{r2} , it had a same value (~ 50 mV) as the calibration voltage at 0 V (first step in Fig. S5a) and remained unchanged, indicating that no heat was generated within r2 segment. For the mixing process, U_{pre} and U_{r2} were the same as in reaction while U_{r1} decreased gradually. Table S3 shows the measured data at 0 °C.

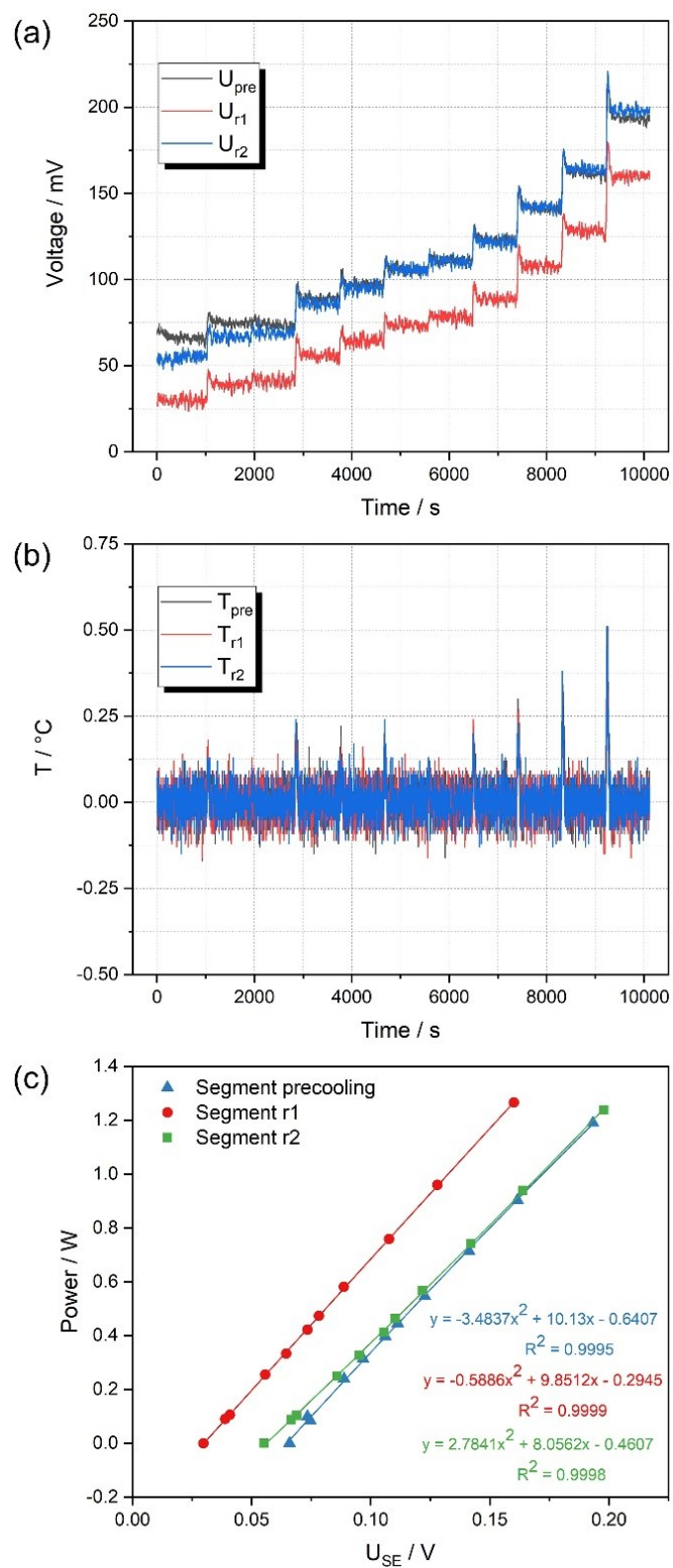


Fig. S5. Calibration of the reactor segments for reaction of HexLi with EtOH at 0 $^\circ\text{C}$: (a) thermoelectric voltages; (b) temperatures; (c) correlations of heat flux and thermoelectric voltage.

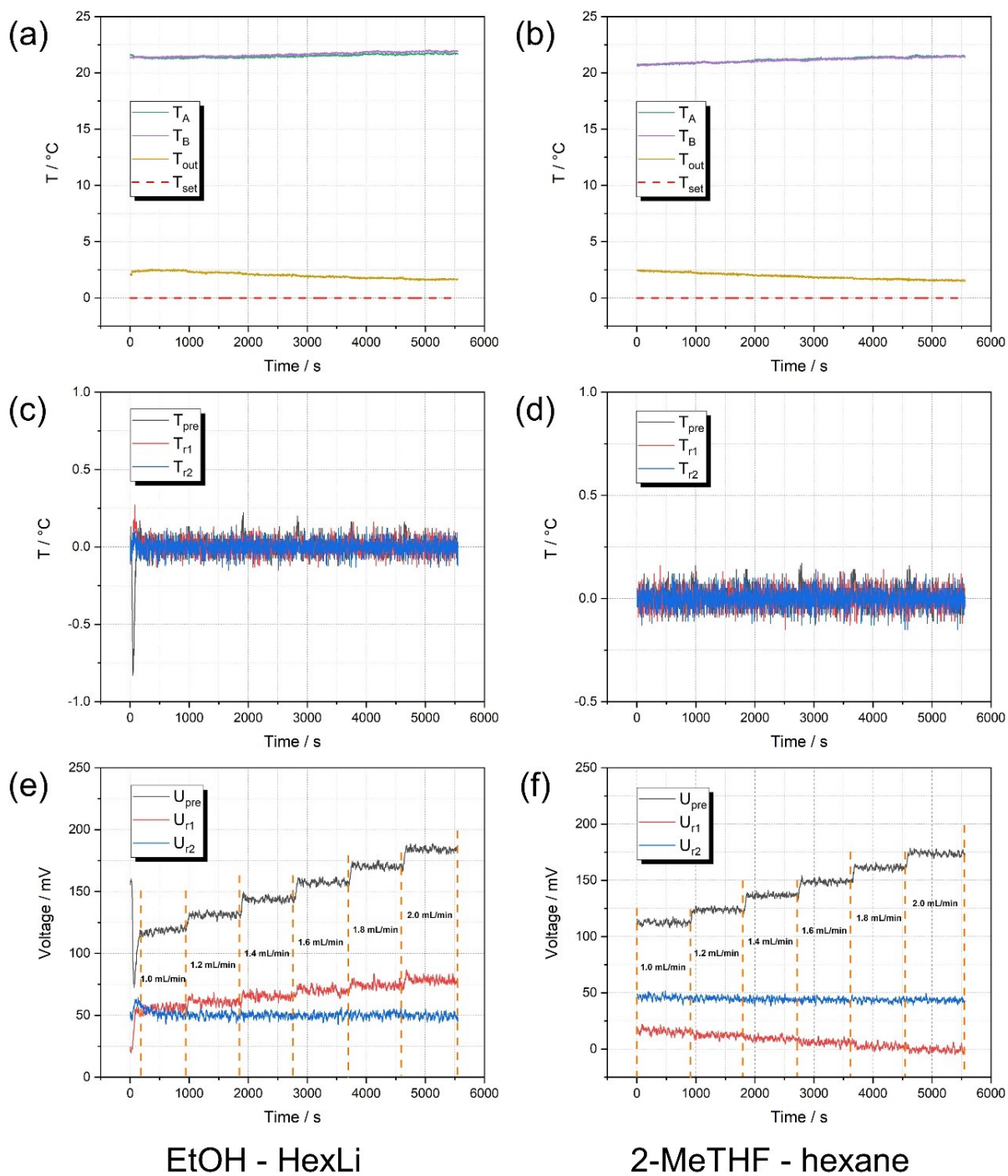


Fig. S6. Reaction of HexLi with EtOH at 0 °C at different total flow rates: (a) temperatures for reaction at inlets and outlet; (b) temperatures for mixing at inlets and outlet; (c) temperatures of the three segments for reaction; (d) temperatures of the three segments for mixing; (e) thermoelectric voltages for reaction; (f) thermoelectric voltages for mixing.

Table S3. Repetitions of calorimetry for reaction of HexLi with EtOH at 0 °C.

Entry	Flow rate [mL/min]		ΔH_r [kJ/mol]	Ave. \pm SD [kJ/mol]
	EtOH in 2-MeTHF	HexLi in hexane		
1	0.52	0.50	-290.4	-301.0 \pm 6.9
	0.63	0.60	-294.6	
	0.73	0.70	-304.2	
	0.83	0.80	-307.1	
	0.94	0.90	-303.2	
	1.04	1.00	-306.3	
2	0.52	0.50	-298.9	-307.1 \pm 11.3
	0.62	0.60	-314.4	
	0.72	0.70	-310.7	
	0.82	0.80	-316.3	
	0.93	0.90	-314.2	
	1.03	1.00	-288.0	

3.3 Batch verification

3.3.1 General procedure

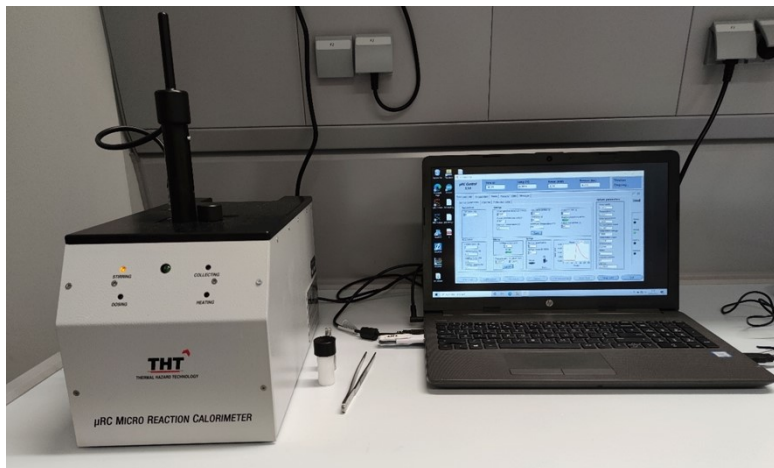


Fig. S7. Image of the μ RC.

A micro reaction calorimeter (μ RC) from Thermal Hazard Technology (THT) was used to collect data to compare to the data collected in the continuous flow calorimeter. The experiment was performed at 25 °C. The HexLi solution was diluted with hexane to 0.5 M. Three different solutions of EtOH were used for comparison, absolute EtOH, 0.5 M EtOH in 2-MeTHF and 0.5 M EtOH in hexane. Although the concentration of reagents was different from those used in flow, it should have no influence on reaction enthalpy.

A titration mode was adopted. 1 mL EtOH solution was added to the reference vial and sample vial, respectively. HexLi solution was loaded into a 100 μ L syringe and used as titrant. For each experiment, injection sizes and number of injections were specified (e.g., 10 μ L \times 10 times, 13 μ L \times 7 times or 15 μ L \times 6 times). The first injection is typically excluded from the calculation as normally the injection volume is smaller than expected. For blank tests, the only difference was that HexLi solution was replaced by hexane. For each condition, the experiment was repeated at least twice to check the consistency. As EtOH was in excess, the calculation of reaction enthalpy was based on HexLi.

3.3.2 Calorimetry results in batch

(1) 0.5 M HexLi in hexane and 0.5 M EtOH in hexane

$\Delta H_r = -271.7 \pm 0.9$ kJ/mol for this condition. The blank test (mixing of hexane and hexane) showed very little heat absorption. This slight difference could have been caused by the difference in the ambient temperature being lower than the set temperature (25 °C). Compared to the reaction enthalpy in the flow calorimeter (-297.6 ± 11.8 kJ/mol), the deviation was 8.7%.

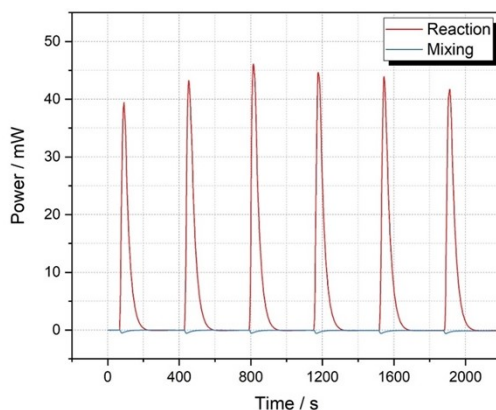


Fig. S8. Calorimetric characterization of the reaction and mixing at 25 °C, HexLi and EtOH both diluted in hexane (0.5 M), 15 μ L/injection \times 6 injection times.

(2) 0.5 M HexLi in hexane and absolute EtOH

ΔH_r values before and after excluding the mixing heat were -236.3 ± 1.8 and -272.4 ± 2.2 kJ/mol, respectively. The blank test (mixing of hexane and absolute EtOH) showed heat absorption which shows that the mixing process is endothermic. When compared to the reaction enthalpy measured in the flow calorimeter, the deviation was 8.4%.

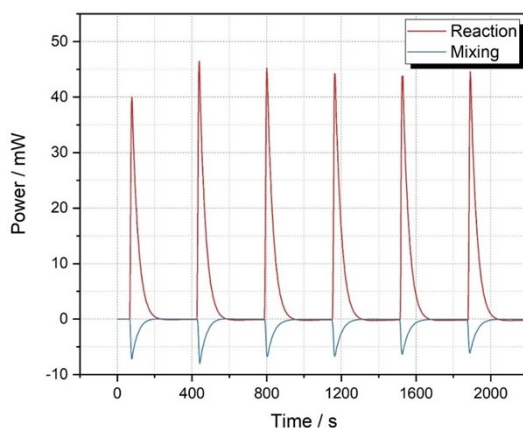


Fig. S9. Calorimetric characterization of the reaction and mixing at 25 °C, HexLi diluted in hexane (0.5 M) and absolute EtOH, 15 μ L/injection \times 6 injection times.

3.3.3 Titration of 2-MeTHF with HexLi

In order to demonstrate the potential reaction between 2-MeTHF and HexLi, a titration experiment was conducted in the micro reaction batch calorimeter. At the beginning, we used 100 μL HexLi (0.5 M) to titrate 1 mL 2-MeTHF in the sample vial ($15 \mu\text{L}/\text{injection} \times 6 \text{ injection times}$). The result is shown in Fig. S10. The detected power for the first four injections were relatively high but it decreased with each subsequent injection. While for the last two injections, the power measured was low. The high values at the beginning may be caused by the reaction between HexLi and moisture in 2-MeTHF. With the dosing of HexLi, there was less moisture and the power decreased. Hence, for the last two injections, the heat could be a result of the reaction between HexLi and 2-MeTHF.

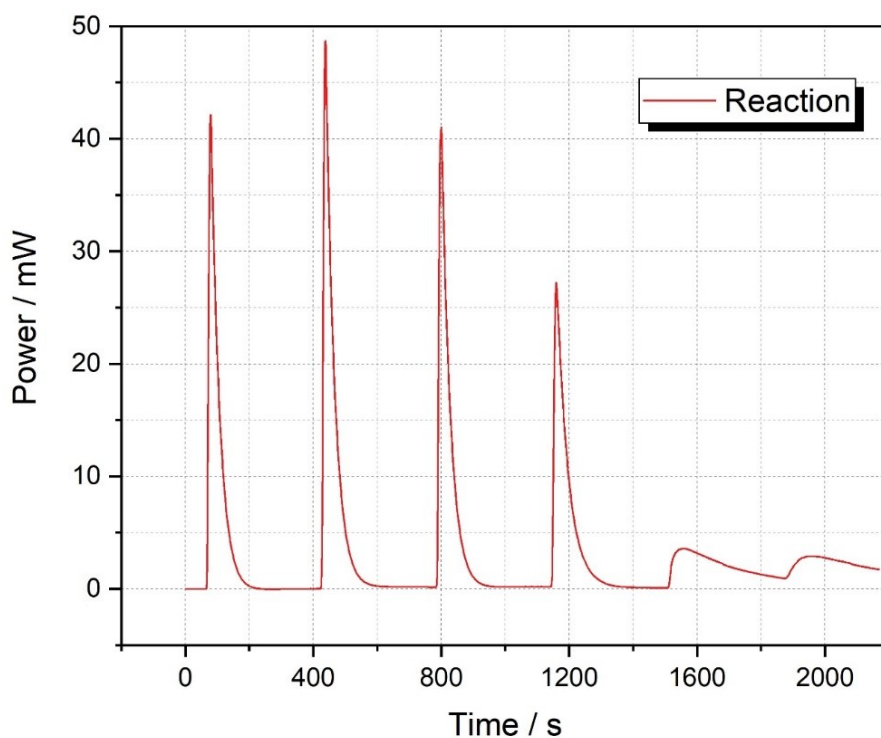


Fig. S10. Thermal behavior of 2-MeTHF titrated with 0.5 M HexLi solution at 25 °C ($15 \mu\text{L}/\text{injection} \times 6 \text{ injection times}$).

For a better demonstration, stock HexLi solution (2.5 M) was used in order to consume the moisture in 2-MeTHF completely at the beginning. The interval time between each injection was prolonged from 300 s to 900 s to ensure that the power decreased to the baseline. The experiment took approximately 3 h. The results are shown in Fig. 6 of the manuscript.

4 Calorimetric characterization for the preparation of tertiary ester 2 and alcohol 3

4.1 General procedure

For the optimization experiments: A solution of (Boc)₂O (**1**) (0.1 M) in 2-MeTHF and a solution of HexLi in hexane were prepared. Before conducting the reaction, the entire flow system was flushed with dry 2-MeTHF and hexane for 20 min and then 10 mL starting solutions. Subsequently, the desired flow rates were set for the two syringe pumps and the reaction commenced. After reaching the steady state ($> 3 \times$ residence time), the effluent was collected and quenched in a vial containing a saturated solution of NH₄Cl (if inline quench was not used). Following extraction with Et₂O (3×10 mL), the collected organic phase was dried over Na₂SO₄, filtered and analysed by GC. After the reaction, dry solvents were used to flush the system.

For the calorimetry experiments: each reaction was run for 20 min and samples were collected at 5, 8, 11, 14, 17, 20 mins. After the reaction, dry solvents were used to run the blank test and to flush the system.

4.2 DoE data

4.2.1 DoE setup

Table S3 shows all the experiments and results obtained from GC analysis. The data were fitted in MODDE (version 12, Umetrics) by using multiple linear regression (MLR), including main terms, interaction terms and square terms. Subsequently, the non-significant terms were all removed.

Table S4. All experiments and results used for DoE analysis.

Entry	Factors			Responses		
	Temperature [°C]	HexLi equiv.	V _{total} [mL/min]	Conversion 1 [%] ^a	Selectivity 2 [%] ^a	Selectivity 3 [%] ^a
1	21	1.10	1.05	66.1	24.9	68.6
2	21	1.10	1.26	67.3	24.8	75.2
3	21	1.10	1.68	67.3	26.1	73.9
4	21	1.10	2.10	74.9	35.5	64.5
5	21	1.10	3.15	80.0	48.7	51.3
6	21	1.10	4.29	75.2	52.2	47.8

7	21	1.10	4.72	77.4	56.1	43.9
8	21	1.10	5.15	79.5	61.5	38.5
9	21	1.10	5.58	79.3	60.9	39.1
10	21	1.15	4.41	77.3	53.1	46.9
11	21	1.15	4.85	80.6	57.3	42.7
12	21	1.15	5.29	82.4	57.7	42.3
13	21	1.15	5.73	84.6	60.6	39.4
14	21	1.20	4.51	80.9	54.5	45.5
15	21	1.20	4.96	83.6	56.6	43.4
16	21	1.20	5.42	85.6	57.3	42.7
17	21	1.20	5.87	87.5	61.4	38.6
18	0	1.10	4.76	80.3	64.8	35.2
19	0	1.10	5.19	82.5	68.9	31.1
20	0	1.10	5.63	83.2	70.6	29.4
21	0	1.10	6.06	85.3	74.8	25.2
22	-10	1.10	5.09	83.4	72.7	27.3
23	-10	1.10	5.51	84.7	75.4	24.6
24	-10	1.10	5.93	85.6	76.3	23.7
25	-10	1.10	6.36	87.1	80.5	19.5
26	0	1.20	4.82	88.0	73.8	26.2
27	0	1.20	5.25	90.7	76.8	23.2
28	0	1.20	5.69	90.3	75.8	24.2
29	0	1.20	6.13	87.0	75.6	24.4
30	0	1.10	4.64	78.8	62.9	37.1
31	0	1.10	5.06	78.1	62.4	37.6
32	0	1.10	5.48	77.4	62.5	37.5
33	0	1.10	5.91	78.8	65.0	35.0
34	0	1.10	6.33	79.5	68.0	32.0
35	0	1.10	6.75	81.0	69.4	30.6
36	0	1.10	7.17	80.9	71.4	28.6
37	-10	1.20	5.25	84.2	68.8	31.2

38	-10	1.20	5.69	86.0	71.5	28.5
39	-10	1.20	6.12	88.0	74.4	25.6
40	0	1.20	5.25	86.0	72.7	27.3
41	0	1.20	5.69	85.3	76.2	23.8
42	0	1.20	6.12	87.8	78.6	21.4

^aDetermined by GC-FID area%.

4.2.2 DoE analysis

Summary of fit for all models: R^2 is a measure of how well the model fits the experimental data points. Q^2 measures how well the model predicts future data (should be greater than 0.1 for a significant model and greater than 0.5 for a good model). Reproducibility is a measure of experimental error. A model validity of above 0.25 indicates a statistically significant model.

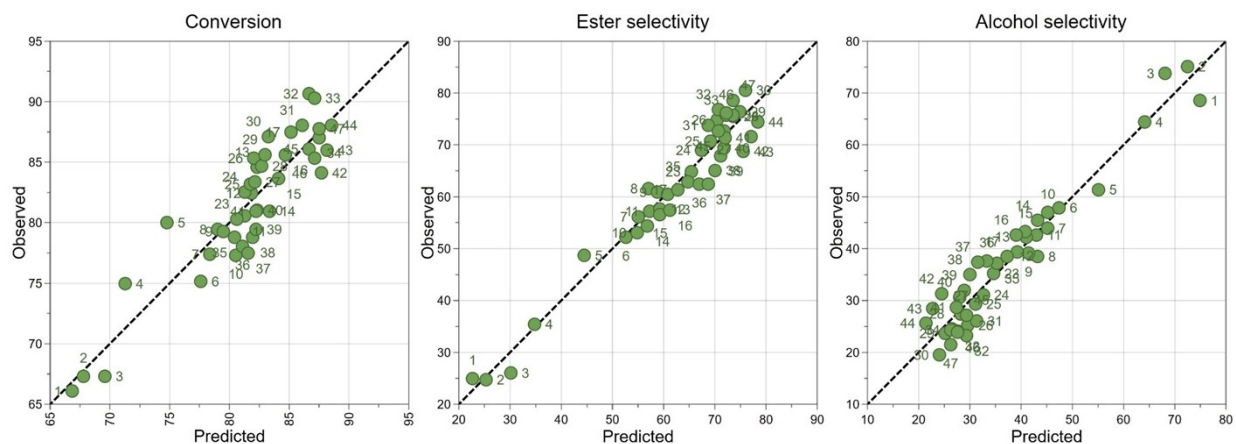


Fig. S11. Observed vs predicted plots from the DoE models.

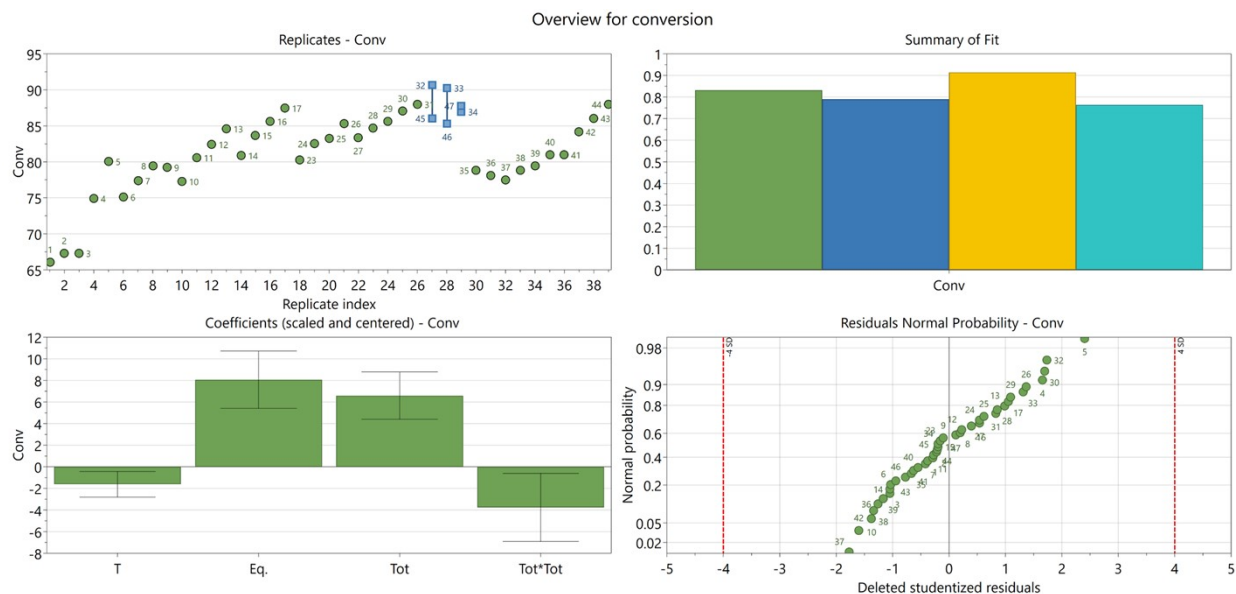


Fig. S12. Model fitting for the conversion of (Boc)₂O (**1**) based on GC-FID data. Top left: replicates plot; Top right: coefficients and terms for model after non-significant terms removed (green R², blue Q², yellow model validity and cyan reproducibility); Bottom left: coefficients with a significant influence (T temperature, Eq. HexLi equivalent, Tot total flow rate, Tot*Tot total flow rate square); Bottom right: residuals normal probability plot.

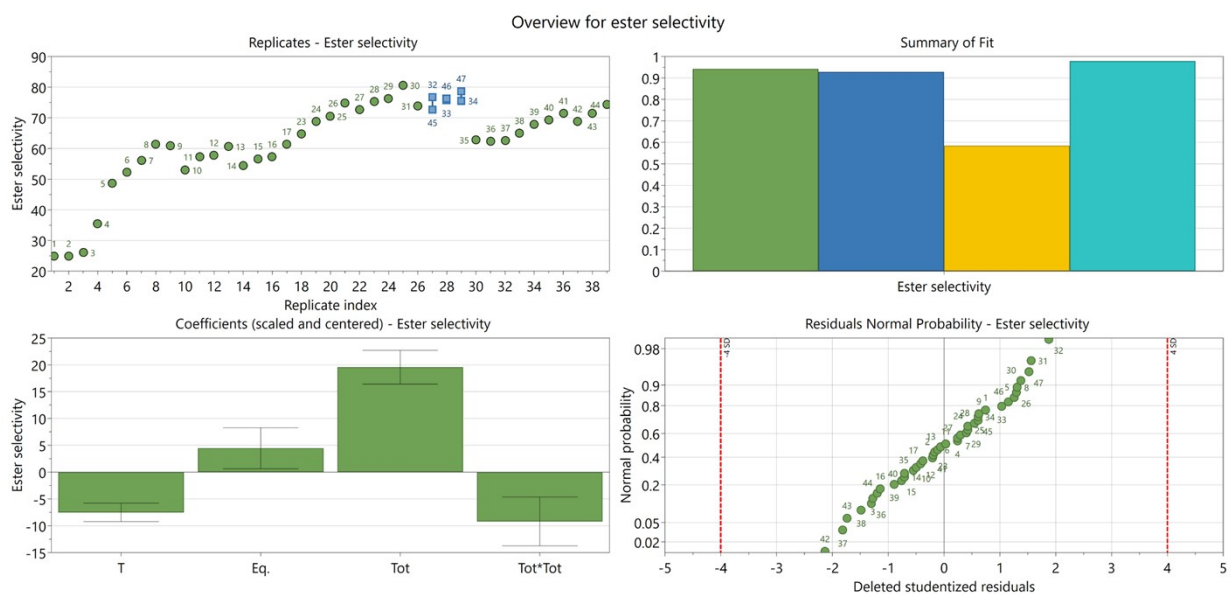


Fig. S13. Model fitting for the selectivity of ester **2** based on GC-FID data. Top left: replicates plot; Top right: coefficients and terms for model after non-significant terms removed (green R^2 , blue Q^2 , yellow model validity and cyan reproducibility); Bottom left: coefficients with a significant influence (T temperature, Eq. HexLi equivalent, Tot total flow rate, Tot* Tot total flow rate square); Bottom right: residuals normal probability plot.

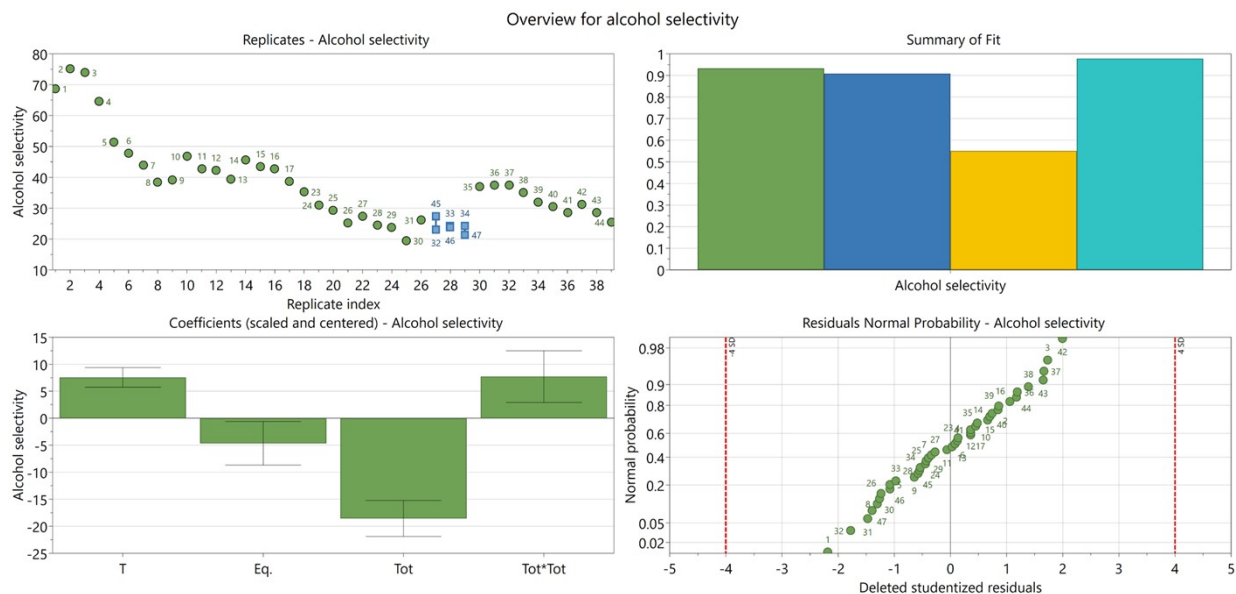


Fig. S14. Model fitting for the selectivity of alcohol **3** based on GC-FID data. Top left: replicates plot; Top right: coefficients and terms for model after non-significant terms removed (green R^2 , blue Q^2 , yellow model validity and cyan reproducibility); Bottom left: coefficients with a significant influence (T temperature, Eq. HexLi equivalent, Tot total flow rate, Tot* Tot total flow rate square); Bottom right: residuals normal probability plot.

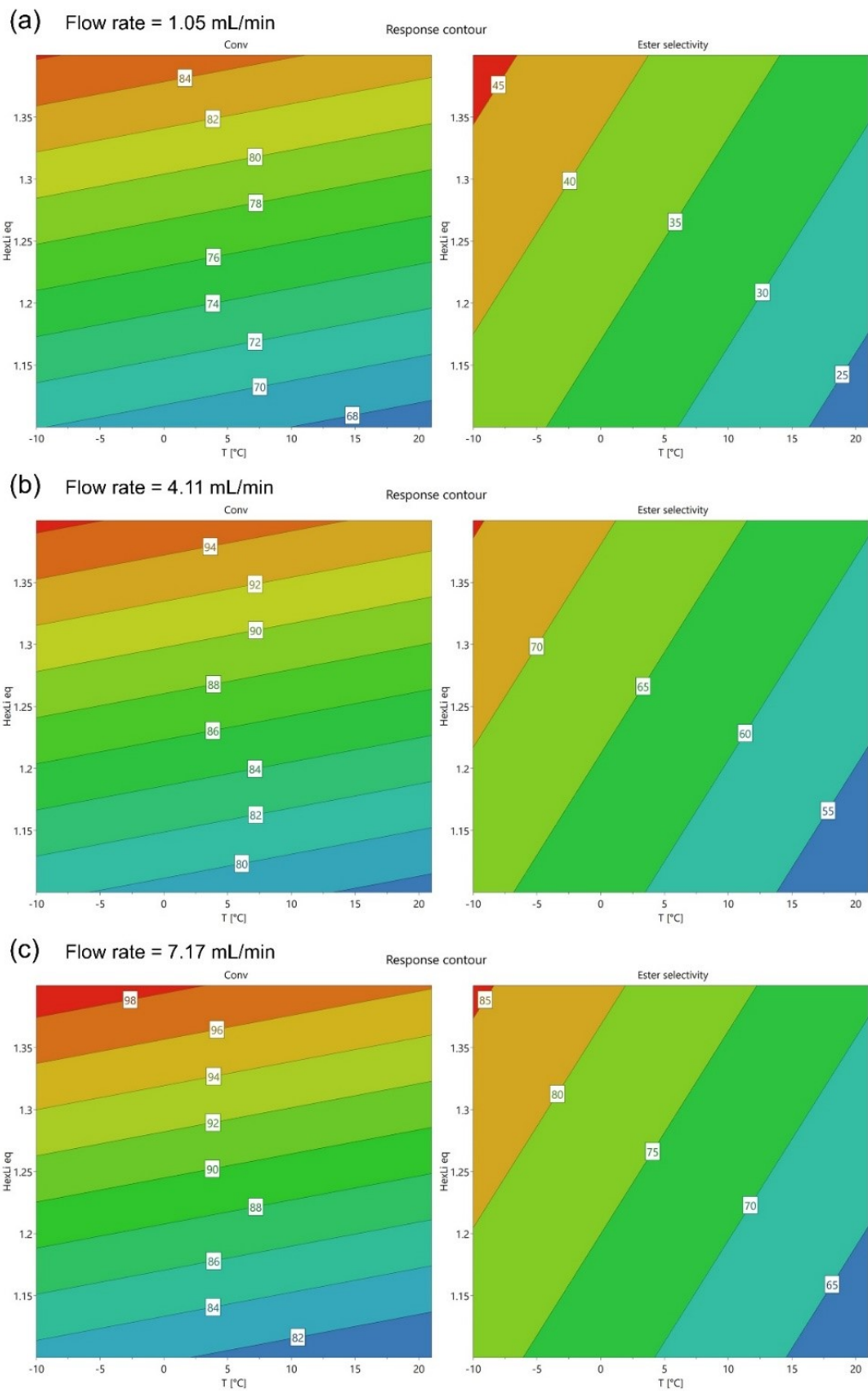


Fig. S15. Contour plots for (Boc)₂O (**1**) conversion and ester **2** selectivity.

4.3 Computational fluid dynamics simulation for solvents mixing

4.3.1 Geometry and governing equations

A 3D representation of the calorimeter was drawn in SolidWorks (Dassault Systèmes S.A.), shown in Fig. S16. It is consistent to the device used experimentally, with the exception that the precooling segment is truncated within the drawing. The channel has a square cross section ($W = H = 0.8 \text{ mm}$) and the length of the inlet part L is $10\times$.

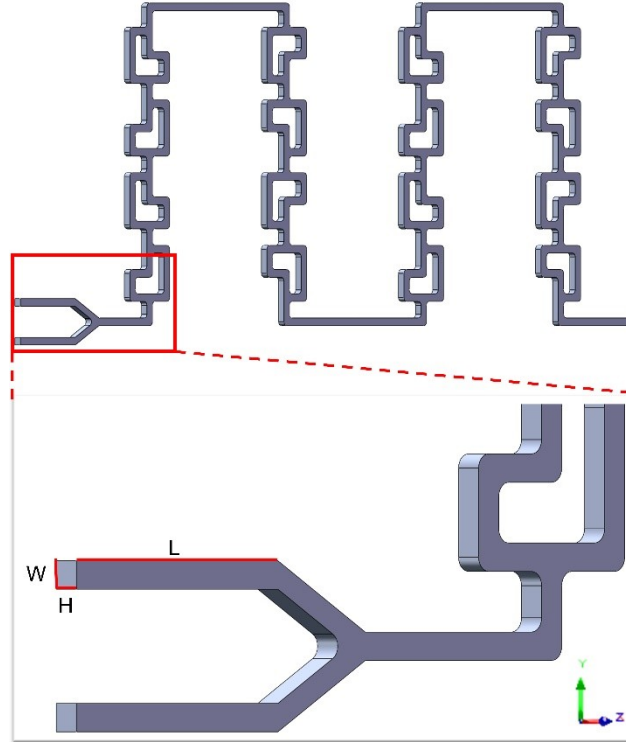


Fig. S16. Schematic diagram of the calorimeter.

The flow of the two streams in the microchannel is considered incompressible and can be described by the Navier-Stokes equation. To simplify the simulation, the mixing process is assumed to be isothermal. In general, the governing equations at steady state are as follows:

$$\nabla \cdot v = 0 \quad (S1)$$

$$\rho v \cdot \nabla v = -\nabla p + \mu \nabla^2 v + \rho g \quad (S2)$$

$$v \nabla \phi = D \nabla^2 \phi \quad (S3)$$

where v is the fluid velocity vector, ρ is the fluid density, p is the static pressure, μ is the fluid dynamic viscosity, g is the gravitational acceleration, ϕ is the mass fraction of one of the two inlet fluids, and D is the molecular diffusivity.

4.3.2 Solution and boundary conditions

Simulations were carried out with the commercial software Fluent 18.2 (Ansys, INC.). The geometry was meshed with Ansys Meshing using sweep method. The physical properties of the two solvents are listed in Table S4. The fluid property of the mixture was estimated using the integrated mixing laws in Fluent. Velocity-inlet and constant atmospheric pressure-outlet were prescribed for the two inlets and the outlet, respectively. As the Reynolds number of the flow in this study ($Re = 38 \sim 234$) was less than 2000, the steady incompressible $N-S$ equation was solved using a laminar model. A no-slip wall was adopted. "Pressure-based solver" was used and gravity was on ($-z$ direction). The Semi-Implicit Method for Pressure Linked Equations (SIMPLE)" algorithm was implemented for pressure velocity coupling while "Green-Gauss Node Based" was for gradient estimation. Pressure discretization was done via "Second order" and "Quick" was adopted for the momentum equation. The absolute convergence criteria of residuals were set to $1E-8$ for all the variables to check the convergence.

Table S5. Physical properties of the solvents (20 °C).

Fluid	Density ρ [kg/m ³]	Viscosity μ [mPa·s]
Hexane	659.38	0.31
2-MeTHF	852.95	0.49

4.3.3 Definition of degree of mixing

The mixing index (MI) represents the degree of homogeneity of two fluids. It ranges from 0 (totally segregated) to 1 (fully mixed). In the numerical simulation, the mixing index is calculated as follows [2]:

$$MI = 1 - \frac{\sigma_b}{\sigma_{max}} \quad (S4)$$

σ_b and σ_{max} indicate the volumetric and maximum flow variance and can be described as follows:

$$\sigma_b = \sqrt{\frac{1}{N\bar{\rho}\bar{u}} \sum_{i=1}^N (\phi_i - \bar{\phi}_b)^2 \rho_i u_i} \quad (S5)$$

$$\sigma_{max} = \sqrt{\bar{\phi}_b(1 - \bar{\phi}_b)} \quad (S6)$$

where N is the number sampling points. ρ_i and u_i are the density and axial velocity at the local position, respectively. $\bar{\rho}$ is the density average and \bar{u} is the velocity average within the cross section.

Due to the non-uniform velocity profile inside the channel, the bulk average mass transfer is calculated as follows:

$$\bar{\phi}_b = \frac{\sum \phi_i \rho_i u_i}{N\bar{\rho}\bar{u}} \quad (S7)$$

4.3.4 Mesh independence

Four different meshes were constructed with the same meshing strategy to test the grid independence. Simulations were run for each mesh with the same solver settings, boundary and initial conditions. The MI at certain cross sections (1, 7, 13, 19, 25) were selected as the variable and the results are shown in Fig. S17. Compared with the finest mesh (mesh 4), the relative discrepancy of MI decreased with the increase of nodes number. Therefore, considering the computational costs and accuracy of the results, mesh 3 was adopted for further calculations.

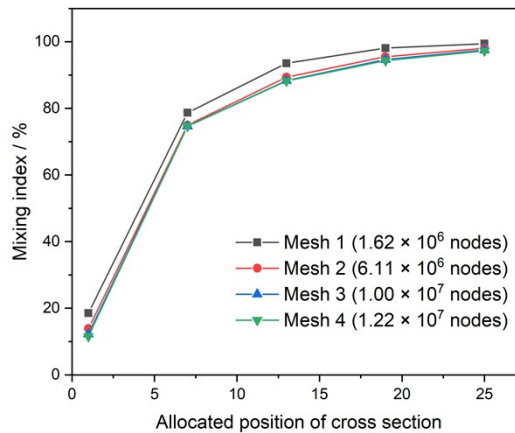


Fig. S17. Mesh independence validation.

4.3.5 Mixing at different flow rates

Diffusion and convection are the two main mechanisms for the mixing of fluids in microchannels. Typical molecular diffusivity of a liquid phase is about 10^{-9} m²/s. As we do not know the diffusion coefficient between 2-MeTHF and hexane, we used $D_{\text{hexane-hexane}}$ (3.9×10^{-9} m²/s) and $D_{\text{THF-THF}}$ (2.4×10^{-9} m²/s) instead. Therefore, before we carried out our simulation, we tried to determine whether the value of diffusivity D would affect the result.

According to Fig. S18, a change of diffusion coefficient strongly affects the MI at the lowest flow rate. This effect gradually diminished with the increase of flow rates, because a convection mechanism dominated the mixing at higher flow rates. This result agreed well with a previous study [3]. Hence, in our simulations, the influence of diffusion coefficient still existed at low flow rates. In the following calculations, $D_{\text{hexane-hexane}}$ was used.

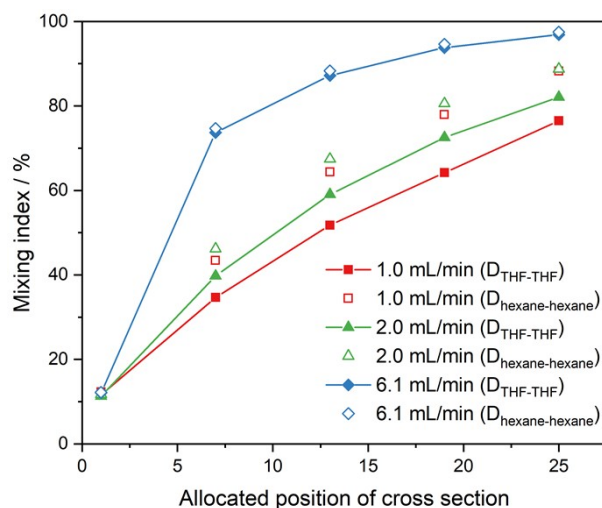


Fig. S18. Effect of diffusion coefficient on mixing index at different flow rates.

Fig. S19 shows the result of the mixing process between 2-MeTHF and hexane at different flow rates. At the flow rate of 1 mL/min, the two solvents remained separated even after four 'split-and-recombine' units. At higher flow rates, the mixing was enhanced due to the stronger convection. Therefore, the mixing of the solvents was faster with higher flow rates which can explain the better selectivity towards the desired ester **2**.

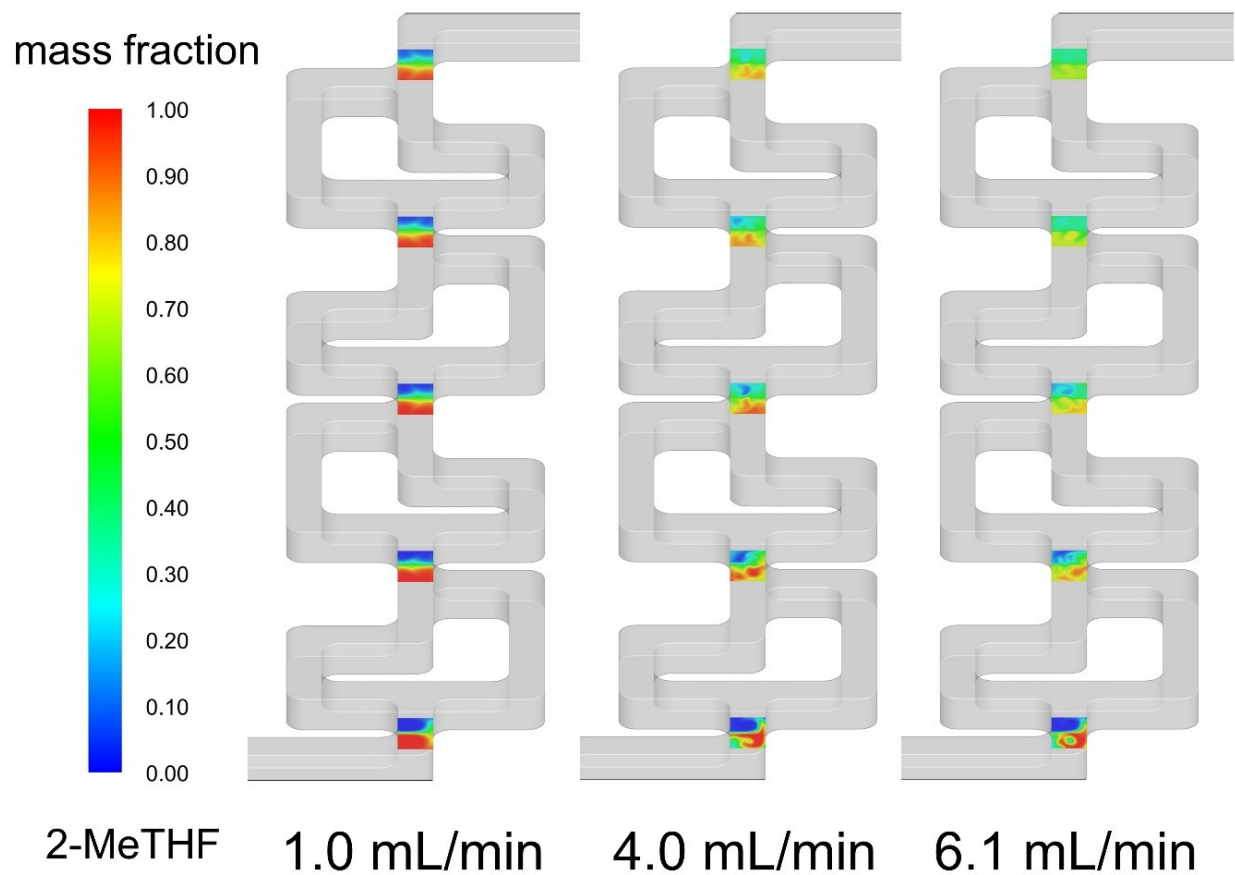


Fig. S19. Phase contour of the mixing process at different flow rates.

This simulation, which demonstrates the mixing process and mixing quality, provides an insight into the reaction between $(\text{Boc})_2\text{O}$ (**1**) and HexLi. However, further studies should be performed to experimentally validate the conclusions regarding the mixing efficiency from the CFD studies.

4.4 Calorimetry data

4.4.1 Calorimetry for preparation of tertiary ester 2

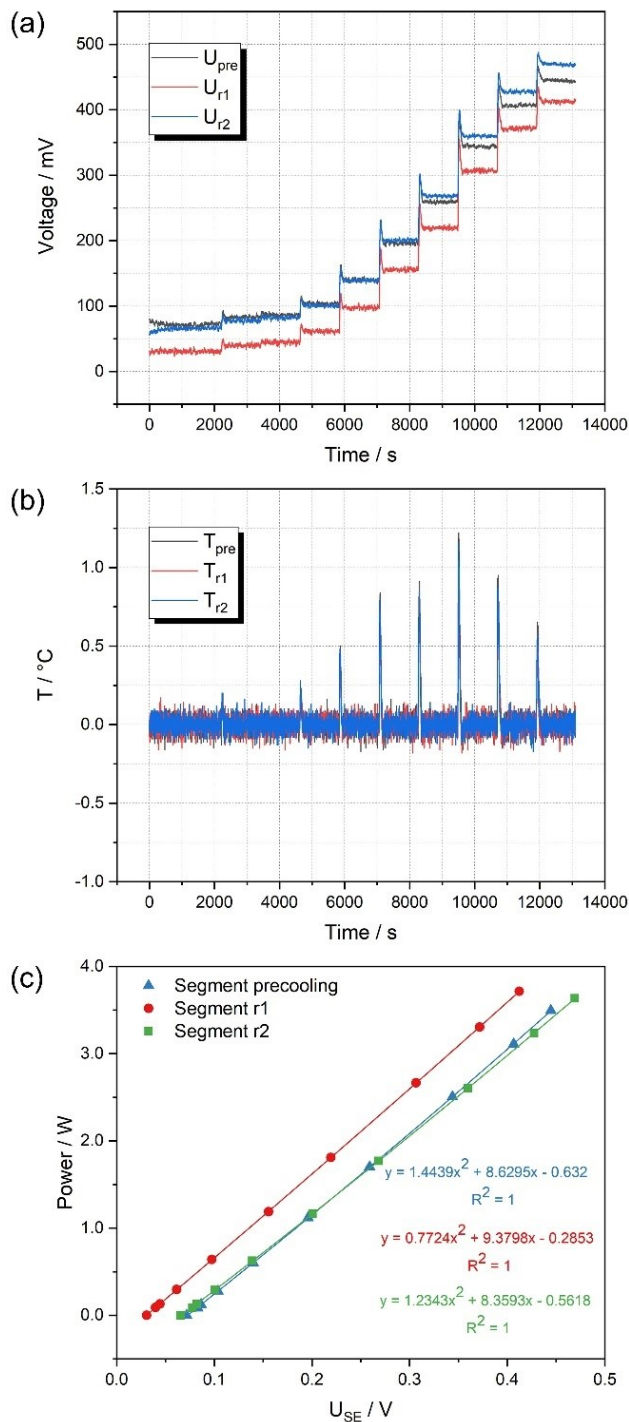


Fig. S20. Calibration of the reactor segments for the preparation of tertiary ester 2 at 0 °C: (a) thermoelectric voltages; (b) temperatures of the three segments; (c) correlations of heat flux and thermoelectric voltage.

Table S6. Summary of reaction enthalpy for preparation of tertiary ester **2** under the optimized condition.

Entry	T [°C]	HexLi equiv. ^a	Residence time [s] ^b	Sampling time [min]	Conv. 1 [%] ^c	Sel. 2 [%] ^c	Sel. 3 [%] ^c	ΔH_r [kJ/mol]	Ave. \pm SD [kJ/mol]
1	0	1.2	3.4	5	89.4	73.4	26.6	-491.5	
				7	90.2	72.6	27.4		
				9	89.2	73.7	26.3		
				11	88.5	73.2	26.8		
				13	89.7	72.4	27.6		
				15	88.6	72.1	27.9		
2	0	1.2	3.4	5	89.3	69.7	30.3	-481.8	-486.7 \pm 6.8
				8	89.6	70.6	29.4		
				11	91.5	73.7	26.3		
				14	90.1	72.4	27.6		
				17	89.2	70.1	29.9		
				20	88.5	70.1	29.9		

^aThe concentration of HexLi solution and (Boc)₂O (**1**) was 0.1 M; ^bBased on two reaction segments (220 μ L) and a 26 cm PFA outlet tubing (i.d. 0.8 mm), 2.8 mL/min for (Boc)₂O (**1**) and 3.3 mL/min for HexLi; ^cDetermined by GC-FID area%.

4.4.2 Calorimetry for preparation of tertiary alcohol 3

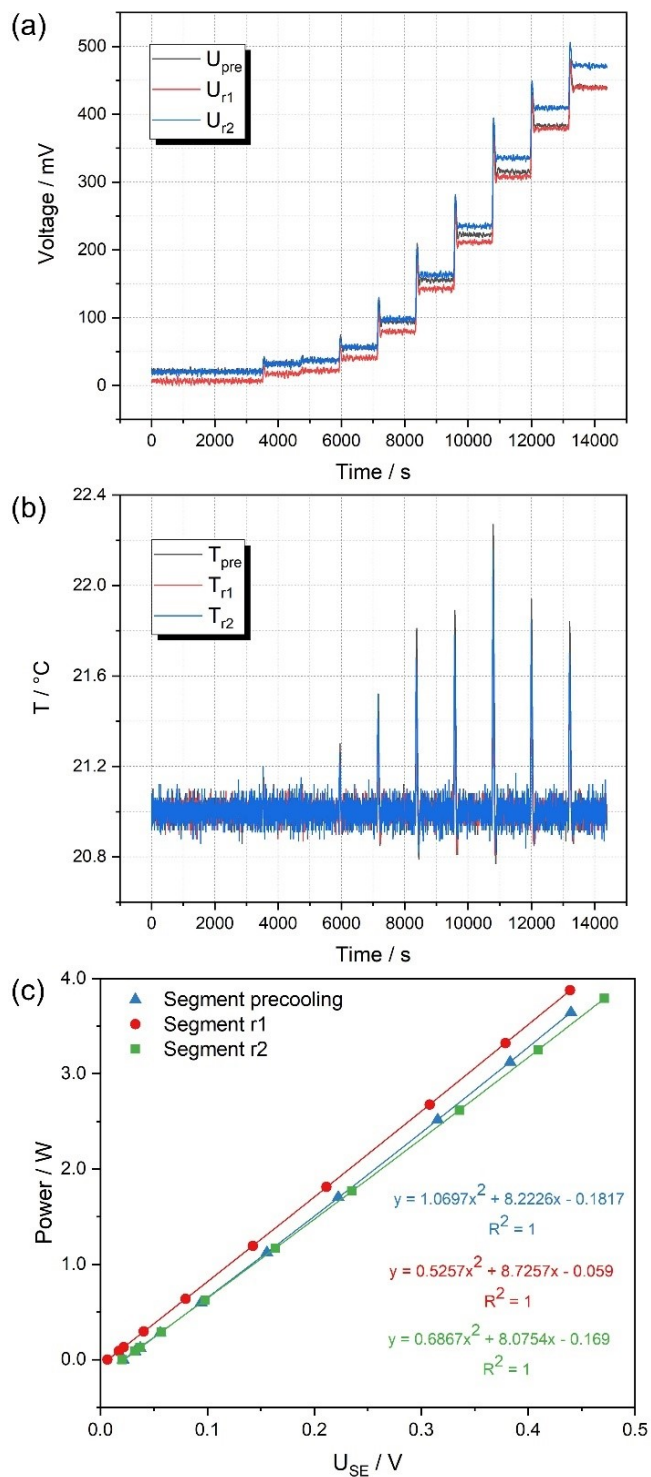


Fig. S21. Calibration of the reactor segments for preparation of tertiary alcohol 3 at 21 $^\circ\text{C}$: (a) thermoelectric voltages; (b) temperatures of the three segments; (c) correlations of heat flux and thermoelectric voltage.

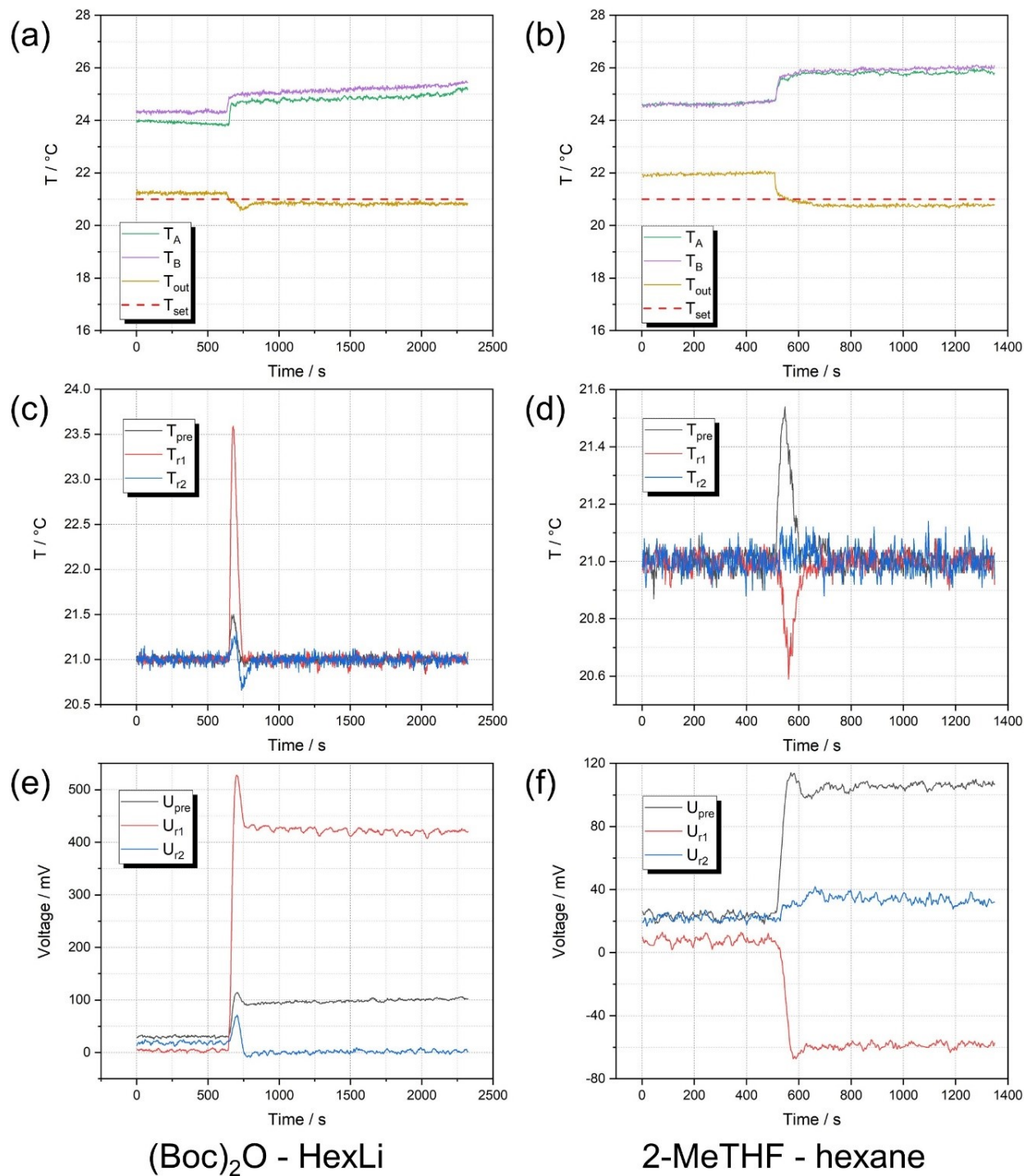


Fig. S22. Calorimetry for preparation of tertiary alcohol **3** at 21 °C: (a) temperatures for reaction at inlets and outlet; (b) temperatures for mixing at inlets and outlet; (c) temperatures of the three segments for reaction; (d) temperatures of the three segments for mixing; (e) thermoelectric voltages for reaction; (f) thermoelectric voltages for mixing.

Table S7. Summary of reaction enthalpy for preparation of tertiary alcohol **3** under the optimized condition.

Entry	T [°C]	HexLi equiv ^a	Residence time [s] ^b	Sampling time [min]	Conv. 1 [%] ^c	Sel. 2 [%] ^c	Sel. 3 [%] ^c	ΔH_r [kJ/mol]	Ave. \pm SD [kJ/mol]
1	21	2.8	3.6	5	100.0	12.8	87.2	-805.6	
				8	100.0	13.1	86.9		
				11	98.4	13.9	86.1		
				14	100.0	12.1	87.9		
				17	100.0	11.5	88.5		
				20	99.5	11.1	88.9		
2	21	2.8	3.6	5	100.0	11.9	88.1	-807.2	-806.4 \pm 1.1
				8	99.7	12.4	87.6		
				11	100.0	10.9	89.1		
				14	100.0	9.6	90.4		
				17	99.7	10.7	89.3		
				20	100.0	9.9	90.1		

^aThe concentration of HexLi solution and (Boc)₂O (**1**) were 0.3 M and 0.1 M, respectively; ^bBased on two reaction segments (220 μ L) and a 26 cm PFA outlet tubing (i.d. 0.8 mm), 3.0 mL/min for (Boc)₂O (**1**) and 2.8 mL/min for HexLi; ^cDetermined by GC-FID area%.

5 Calorimetric characterization of Br–Li exchange and its quench with I₂

5.1 General procedure

For the optimization experiments: A solution of 1-bromo-4-chlorobenzene (**5**) in 2-MeTHF, a solution of I₂ in 2-MeTHF and a solution of HexLi in hexane were prepared, respectively. Before conducted the reaction, the whole system was flushed with dry 2-MeTHF and hexane for 20 mins and then 10 mL starting solutions. After that, desired flow rates were set to the three syringe pumps and the reaction began. After reaching the steady state ($> 3 \times$ residence time), the out-coming solution was collected in a vial containing a saturated solution of NH₄Cl. Following extraction with EtOAc (3×10 mL), the collected organic phase was dried over Na₂SO₄, filtered and analysed by GC. After the reaction, dry solvents were used to flush the system.

If inline quench was not used, the sample was collected in a sealed vial containing a solution of I₂ and stirred for 30 mins. Then the resulting solution was transferred to the NH₄Cl solution, followed by extraction, drying and analysis.

For the calorimetry experiments: The reaction was run for 20 mins and samples were collected at 5, 8, 11, 14, 17, 20 mins. After the reaction, dry solvents were used to run the blank test and flush the system.

Note: A T-piece was used directly after the outlet port for introducing the quench feed instead of the quenching port on the calorimeter. We found that if the quench port was used, it may have some influence on the calorimetry measurements due to heat conduction. Thus, the use of a T-piece immediately after the calorimeter can avoid this potential influence.

5.2 Calorimetry data

5.2.1 Calorimetry for Br–Li exchange

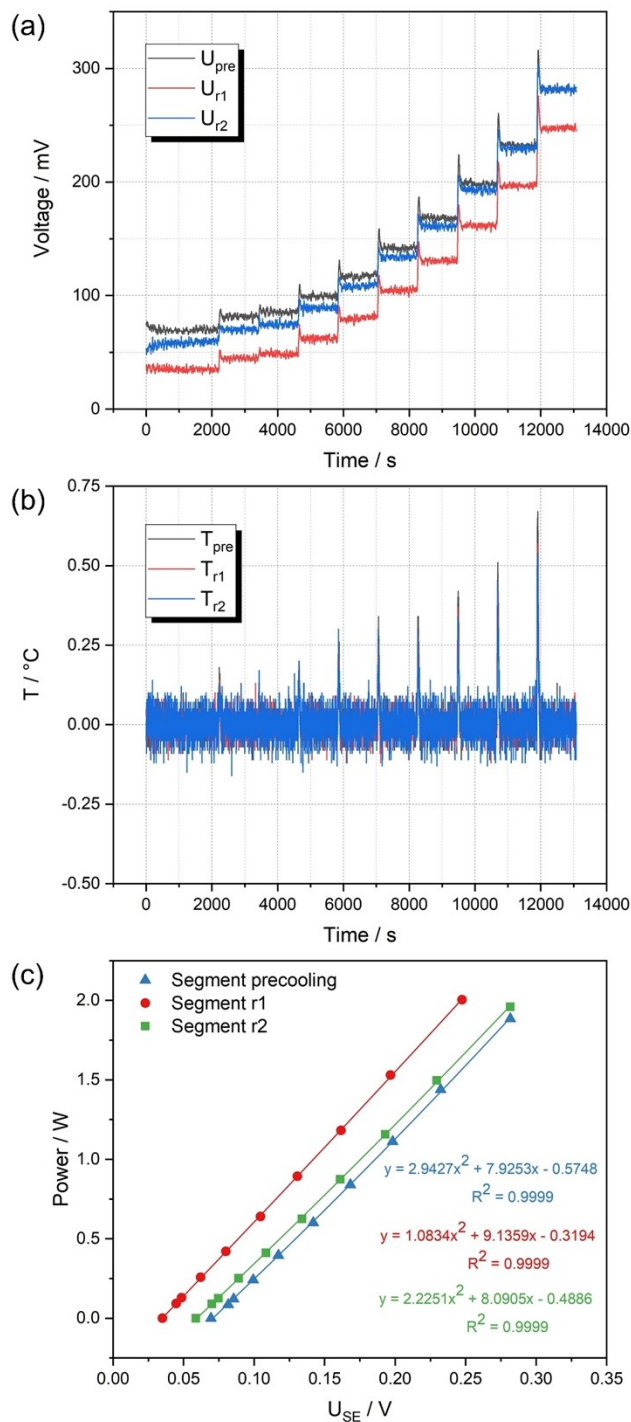


Fig. S23. Calibration of the reactor segments for Br–Li exchange at 0 °C: (a) thermoelectric voltages; (b) temperatures of the three segments; (c) correlations of heat flux and thermoelectric voltage.

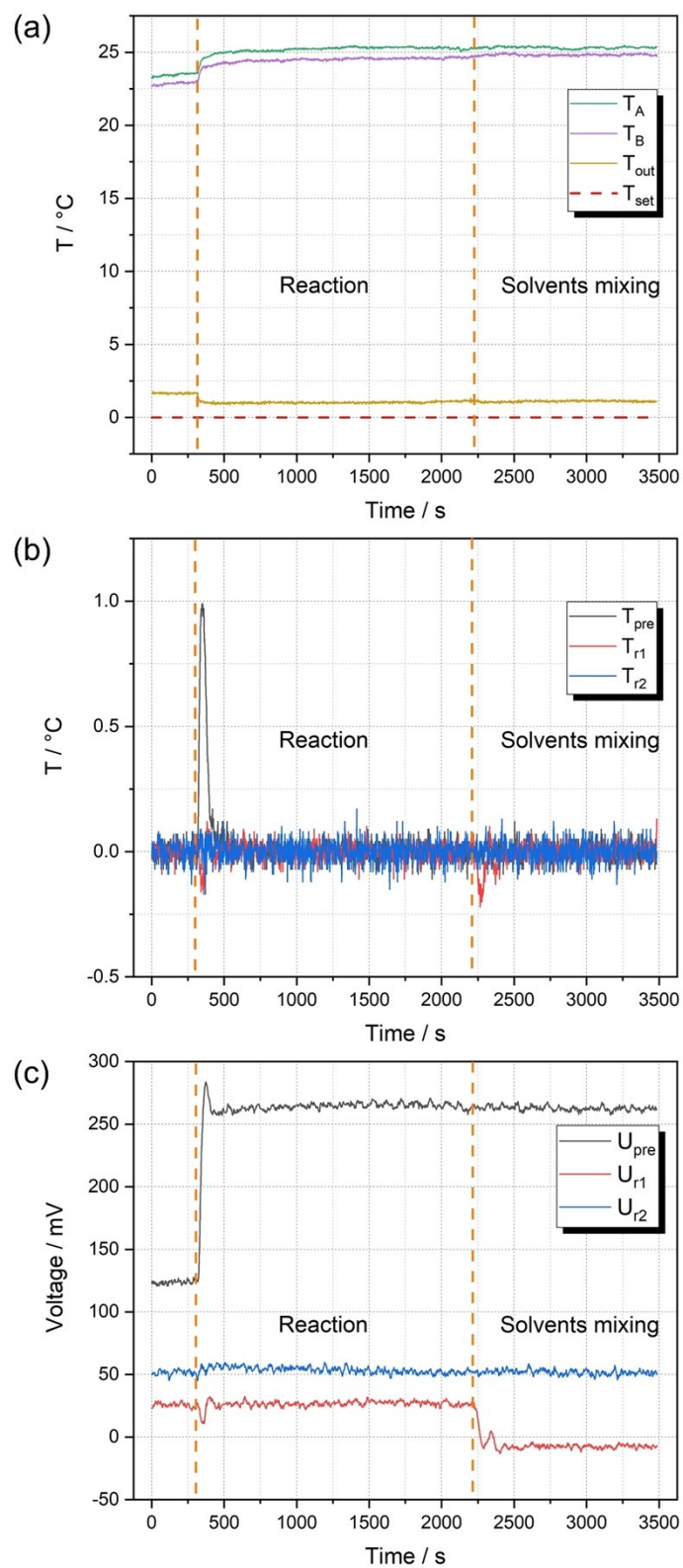


Fig. S24. Calorimetry for Br–Li exchange at 0 °C: (a) temperatures at inlets and outlet; (b) temperatures of the three segments; (c) thermoelectric voltages.

Table S8. Summary of reaction enthalpy for Br–Li exchange under the optimized condition.

Entry	T [°C]	HexLi equiv ^a	t ^{R1} [s] ^b	Sampling time [min]	Conv. 5 [%] ^c	Sel. 7 [%] ^c	Sel. 8 [%] ^c	ΔH_r [kJ/mol]	Ave. \pm SD [kJ/mol]
1	0	1.1	4.4	5	84.9	85.7	14.3	-157.3	
				8	84.0	85.9	14.1		
				11	82.5	85.7	14.3		
				14	82.3	85.7	14.3		
				17	81.6	85.7	14.3		
				20	81.2	84.7	15.3		
2	0	1.1	4.4	5	87.5	87.8	12.2	-146.0	-151.7 \pm 8.0
				8	88.1	87.7	12.3		
				11	89.9	87.3	12.7		
				14	91.5	87.7	12.3		
				17	92.6	86.7	13.3		
				20	96.6	82.2	17.8		

^aThe concentration of HexLi solution was 0.11M and 1-bromo-4-chlorobenzene (**5**) was 0.10 M; ^bBased on two reaction segments (220 μ L), 1.50 mL/min for 1-bromo-4-chlorobenzene (**5**) and HexLi, respectively; ^cDetermined by GC-FID area%.

5.2.2 Calorimetry for quench of lithiated intermediate 6 with I₂

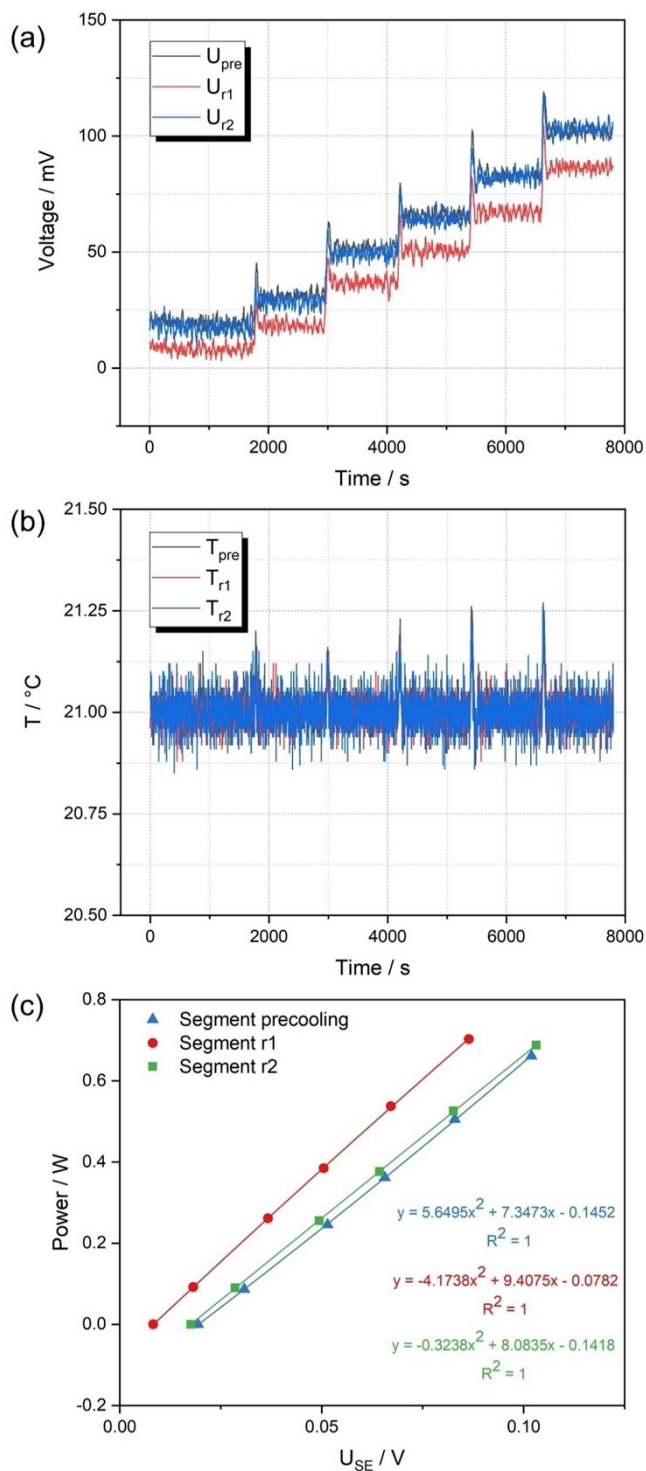


Fig. S25. Calibration of the reactor segments for quench of lithiated intermediate 6 at 21 °C: (a) thermoelectric voltages; (b) temperatures of the three segments; (c) correlations of heat flux and thermoelectric voltages.

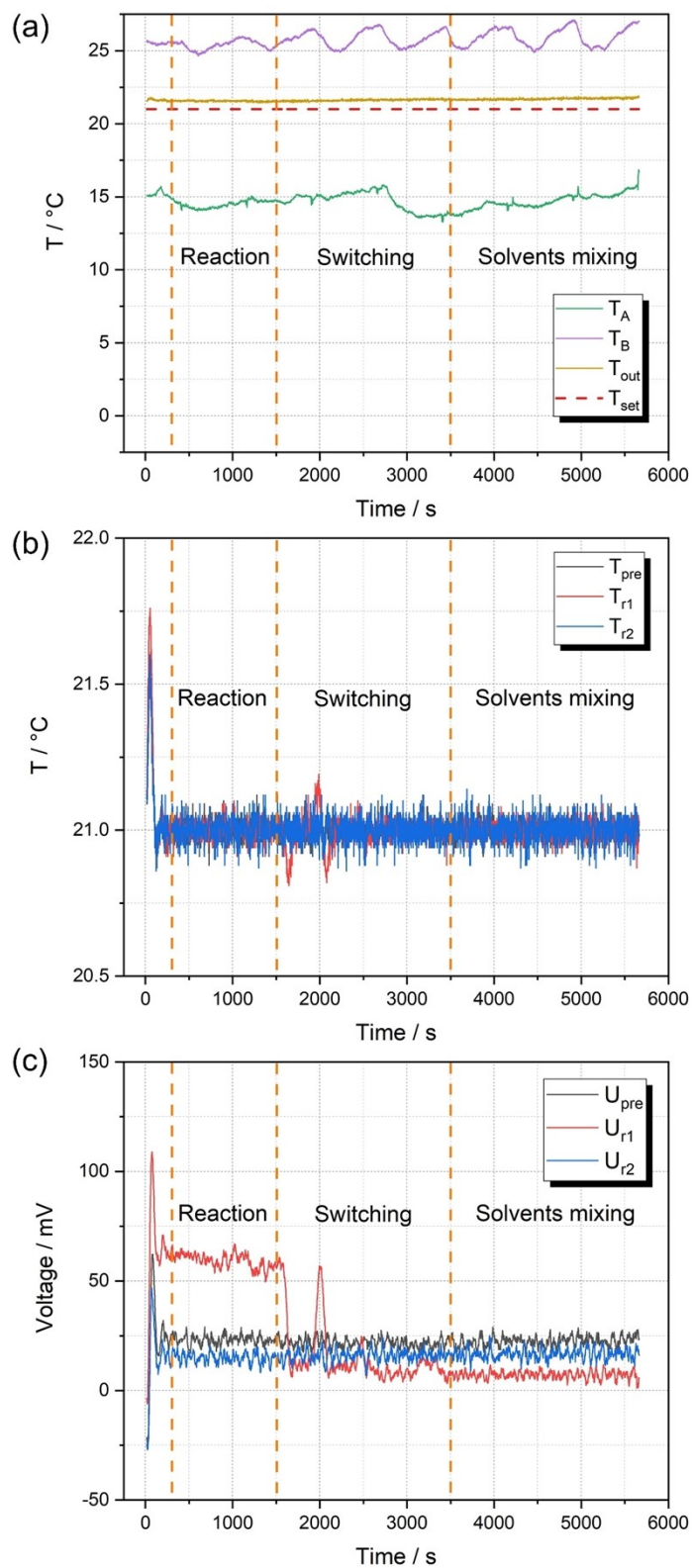


Fig. S26. Calorimetry for quench of lithiated intermediate **6** at 21 $^\circ\text{C}$: (a) temperatures at inlets and outlet; (b) temperatures of the three segments; (c) thermoelectric voltages.

Table S9. Summary of reaction enthalpy for quench of lithiated intermediate **6** with I₂ under the optimized condition.

Entry	T [°C]	HexLi equiv ^a	I ₂ equiv ^b	t ^{R3} [s] ^c	t ^{R4} [s] ^d	Sampling time [min]	Conv. 5 [%] ^e	Sel. 7 [%] ^e	Sel. 8 [%] ^e	ΔH _r [kJ/mol]	Ave. ± SD [kJ/mol]
1	21	1.0	2.0	103.7	17.8	5	83.7	91.8	8.2	-334.5	
						8	84.7	91.1	8.9		
						11	83.7	90.0	10.0		
						14	84.5	90.0	10.0		
						17	85.1	89.5	10.5		
						20	83.7	91.8	8.2		
2	21	1.0	2.0	103.7	17.8	5	88.8	91.1	8.9	-351.1	-342.8 ± 11.7
						8	85.4	90.5	9.5		
						11	89.0	90.4	9.6		
						14	89.9	90.0	10.0		
						17	89.7	90.0	10.0		
						20	88.8	91.1	8.9		

^aThe concentration of HexLi and 1-bromo-4-chlorobenzene (**5**) were 0.50 M; ^bThe concentration of I₂ was 0.60 M; ^cPFA tubing 137.5 cm (0.8 mm i.d.), the flow rate of HexLi and 1-bromo-4-chlorobenzene (**5**) was 0.20 mL/min, respectively; ^dBased on two reaction segments (220 μL), 0.34 mL/min for I₂; ^eDetermined by GC-FID area%.

References

- [1] M.C. Maier, M. Leitner, C.O. Kappe, H. Gruber-Woelfler, A modular 3D printed isothermal heat flow calorimeter for reaction calorimetry in continuous flow, *Reaction Chemistry and Engineering*. 5 (2020) 1410–1420. <https://doi.org/10.1039/d0re00122h>.
- [2] A. Haghghinia, S. Movahedirad, A.K. Rezaei, N. Mostoufi, On-chip mixing of liquids with high-performance embedded barrier structure, *International Journal of Heat and Mass Transfer*. 158 (2020) 119967. <https://doi.org/10.1016/j.ijheatmasstransfer.2020.119967>.
- [3] A. Haghghinia, S. Movahedirad, Fluid micro-mixing in a passive microchannel: Comparison of 2D and 3D numerical simulations, *International Journal of Heat and Mass Transfer*. 139 (2019) 907–916. <https://doi.org/10.1016/j.ijheatmasstransfer.2019.05.084>.